Cell

Transient RNA-DNA Hybrids Are Required for Efficient Double-Strand Break Repair

Graphical Abstract

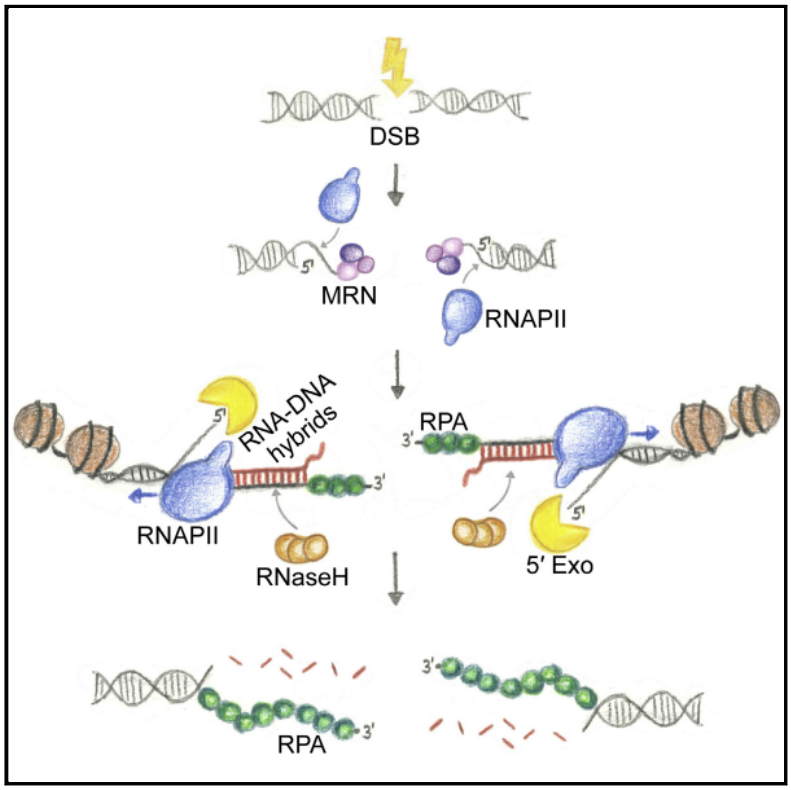

Authors

Corina Ohle, Rafael Tesorero, Géza Schermann, Nikolay Dobrev, Irmgard Sinning, Tamás Fischer

Correspondence

tamas.fischer@anu.edu.au

In Brief

RNA-DNA hybrids, which have previously been associated with genome instability, function as transient intermediates during double-strand break repair and are key for maintenance of genomic integrity.

Highlights

- Deletion or overexpression of RNase H inhibits HR-mediated DSB repair in *S pombe*
- RNA polymerase II and RNA-DNA hybrids are enriched around DSB sites
- Stabilization of RNA-DNA hybrids impairs RPA recruitment to ssDNA overhangs
- RNA-DNA hybrids are essential for maintaining repetitive DNA regions around DSBs

Ohle et al., 2016, Cell *167*, 1001–1013
November 3, 2016
http://dx.doi.org/10.1016/j.cell.2016.10.001

CellPress

Article

Cell

Transient RNA-DNA Hybrids Are Required for Efficient Double-Strand Break Repair

Corina Ohle,[1,3] Rafael Tesorero,[1,3] Géza Schermann,[1] Nikolay Dobrev,[1] Irmgard Sinning,[1] and Tamás Fischer[1,2,4,*]
[1]Heidelberg University Biochemistry Center (BZH), Im Neuenheimer Feld 328, 69120 Heidelberg, Germany
[2]The John Curtin School of Medical Research, The Australian National University, Canberra ACT 2601, Australia
[3]Co-first author
[4]Lead Contact
*Correspondence: tamas.fischer@anu.edu.au
http://dx.doi.org/10.1016/j.cell.2016.10.001

SUMMARY

RNA-DNA hybrids are a major internal cause of DNA damage within cells, and their degradation by RNase H enzymes is important for maintaining genomic stability. Here, we identified an unexpected role for RNA-DNA hybrids and RNase H enzymes in DNA repair. Using a site-specific DNA double-strand break DSB) system in *Schizosaccharomyces pombe*, we showed that RNA-DNA hybrids form as part of the homologous-recombination HR)-mediated DSB repair process and that RNase H enzymes are essential for their degradation and efficient completion of DNA repair. Deleting RNase H stabilizes RNA-DNA hybrids around DSB sites and strongly impairs recruitment of the ssDNA-binding RPA complex. In contrast, overexpressing RNase H1 destabilizes these hybrids, leading to excessive strand resection and RPA recruitment and to severe loss of repeat regions around DSBs. Our study challenges the existing model of HR-mediated DSB repair and reveals a surprising role for RNA-DNA hybrids in maintaining genomic stability.

INTRODUCTION

The integrity of the eukaryotic genome is continuously challenged by external factors, such as UV light, ionizing radiation, or DNA-damaging chemicals, but also by endogenous factors, including reactive oxygen species and replication- or transcription-related events. The DNA repair machinery identifies and repairs damaged DNA and ensures that the genetic information is maintained. Defects in DNA-damage signaling or repair can lead to cancer development and various developmental, immunological, and aging-related diseases (Vijg and Suh, 2013). Among the different types of DNA damage, DNA double-strand breaks (DSBs) are the most deleterious, as they affect both strands of the DNA helix, and their inefficient or inaccurate repair can give rise to genome rearrangements, chromosomal translocations, and cell death. The basic mechanisms for the repair of DSBs have been extensively characterized over the past decades and have been found to be conserved from yeast to humans (Chapman et al., 2012; Mimitou and Symington, 2009; Blackwood et al., 2013).

DSBs can be repaired through two pathways: either the quick but error-prone non-homologous end joining (NHEJ) pathway or the more accurate homologous-recombination (HR) pathway. HR-mediated DSB repair requires the presence of sister chromatids, which restricts this pathway to cells in G2 or S phase. In this pathway, DSBs are detected by the highly conserved Mre11-Rad50-Nbs1/Xrs2 (MRN/MRX) complex, which activates the checkpoint kinase ATM (ataxia telangiectasia mutated). ATM rapidly phosphorylates various DNA repair factors and initiates a global DNA damage response (DDR) in the cell. The MRN/MRX complex, together with Sae2, is also responsible for the initial resection of the DSB ends, generating short, single-stranded 3 overhangs (Mimitou and Symington, 2009; Blackwood et al., 2013). Subsequent long-range resection of the 5 strand is performed by the 5 -3 exonuclease Exo1 or the Dna2-Sgs1/BLM complex (Mimitou and Symington, 2008; Zhu et al., 2008; Blackwood et al., 2013). The long, single-stranded DNA (ssDNA) overhangs that are generated are bound and protected by the trimeric replication protein A (RPA) complex. Subsequently, with the help of Rad52/BRCA2, the RPA complex is replaced by the Rad51 recombinase, forming long nucleoprotein filaments. These Rad51 filaments are essential for the homology search and strand invasion into the undamaged sister chromatid and for the completion of the DNA repair process.

Recent data suggest that non-coding RNAs (ncRNAs) also play a role in the DNA repair process (Chowdhury et al., 2013; Ohsawa et al., 2013). Small ncRNAs were detected in the vicinity of DSBs in various organisms (Lee et al., 2009; Wei et al., 2012; Francia et al., 2012), and it was proposed that they function in the DDR by directing chromatin modifications and other protein complexes to the DSB sites. The production and function of these 20- to 21-nt short ncRNAs are mediated by key RNAi factors, such as the Dicer, Drosha, and Argonaute proteins (Chowdhury et al., 2013). In addition to the recruitment of various factors, RNA can also serve as a template for DSB repair, as was recently reported in *S. cerevisiae* (Keskin et al., 2014).

RNA transcripts can also negatively affect genomic stability by re-annealing to their template DNA strand. The resulting RNA-DNA hybrid and the displaced ssDNA segment is called the R-loop structure. R-loops are highly deleterious for genome integrity, as they can block transcription and DNA replication,

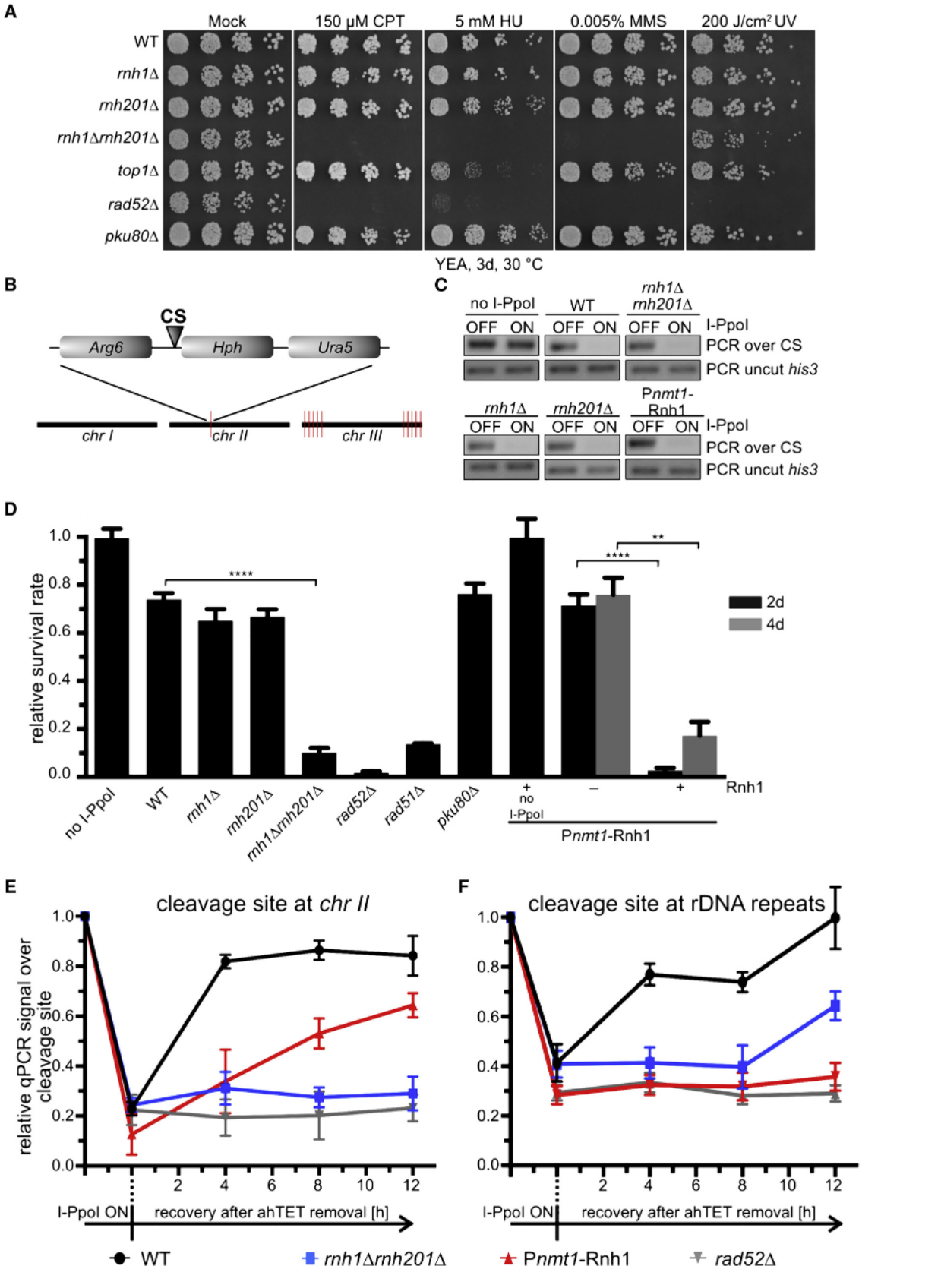

legend on next page)

resulting in replicative stress and the formation of DSBs (Aguilera and García-Muse, 2012; Helmrich et al., 2013). To avoid the formation of R-loops, eukaryotic cells co-transcriptionally package the nascent RNA transcripts into ribonucleoprotein particles (RNPs) and quickly export them to the cytoplasm. Impaired packaging or nucleo-cytoplasmic export leaves unprotected RNA transcripts in the nucleus and leads to increased levels of R-loop formation and genomic instability.

The RNase H family of enzymes can degrade R-loops by cleaving the RNA moiety of the RNA-DNA hybrid in a sequence-independent manner. Eukaryotic cells possess two types of RNase H enzymes; RNase H1 is monomeric, while RNase H2 is a heterotrimeric complex consisting of the catalytic subunit Rnh201 and two auxiliary subunits, Rnh202 and Rnh203. While RNase H2 enzymes can cleave a single ribonucleotide embedded in a DNA duplex, RNase H1 requires a minimum of four consecutive ribonucleotides. However, both types of RNase H enzymes can degrade extended RNA-DNA hybrid structures, typically found in R-loops (Cerritelli and Crouch, 2009). In addition to degrading R-loops, RNase H activity is also involved in eliminating RNA primers and mis-incorporated ribonucleotides during the DNA replication process. In mammals, RNase H1 is indispensable for embryonic development and mtDNA replication (Cerritelli et al., 2003), and mutations in any of the RNase H2 subunits have been associated with the neuroinflammatory disease Aicardi-Goutières syndrome (AGS) (Crow et al., 2006). Interestingly, RNase H activity is not required for cell survival in bacteria and in simple eukaryotic organisms, and our understanding of the in vivo functions of these evolutionarily highly conserved enzymes is still preliminary.

Here, we show that RNase H activity is essential for the efficient repair of DSBs in the fission yeast *Schizosaccharomyces pombe* (*S. pombe*). Deletion of RNase H1 and RNase H2, or overexpression of RNase H1, resulted in the inhibition of HR-mediated DSB repair. Using a site-specific DSB system, we showed the recruitment of RNA polymerase II (Pol II) and the formation of RNA-DNA hybrids around the DSB site. These hybrids were stabilized in cells lacking RNase H activity, leading to strongly impaired recruitment of the ssDNA-binding RPA complex around the DSB site. Overexpression of RNase H1 had the opposite effect, eliminating RNA-DNA hybrids around the DSB and inducing excessive strand resection and RPA recruitment over a longer distance from the DSB site. As a consequence, under conditions of RNase H1 overexpression, repetitive DNA regions around DSBs became destabilized, which particularly affects the highly repetitive rDNA locus. Our results suggest that the appearance of short ssDNA segments around DSB sites induce Pol II transcription and RNA-DNA hybrid formation, and these hybrids are involved in regulating the strand resection process and the recruitment of RPA complex around DSB sites. RNase H activity is subsequently required to degrade these RNA-DNA intermediates and allow the completion of the DSB repair process.

RESULTS

RNase H Activity Is Required for HR-Mediated DSB Repair in *S. pombe*

To further understand the in vivo functions of RNase H enzymes, we analyzed the growth behavior and DNA-damage sensitivity of *S. pombe* strains lacking RNase H1 and/or RNase H2. Neither the single-deletion strains (*rnh1* and *rnh201*) nor the double-deletion strain (*rnh1 rnh201*) showed a significant growth defect, indicating that, under normal growth conditions, RNase H activity is not critical for cell survival in *S. pombe*. However, RNase H activity becomes essential if the cells are exposed to genotoxic drugs that cause DSBs, such as camptothecin (CPT), hydroxyurea (HU), or methyl methanesulfonate (MMS) (Figure 1A). The strong DSB sensitivity observed for the *rnh1 rnh201* strain was not detected in the *rnh1* or the *rnh201* single-deletion strains, suggesting that the two types of RNase H enzymes work redundantly in this process. Since the structural similarity between Rnh1 and the trimeric Rnh201-202-203 complex is limited to the catalytic (RNase H) domain, the strong DNA-damage sensitivity observed in the double-deletion strain can be attributed to the lack of RNase H activity in the cell. Interestingly, while the lack of topoisomerase 1 enzyme (Top1) is known to cause strong genomic instability, the *top1* strain shows only mild sensitivity to DNA-damaging agents. The strong DSB sensitivity observed for the *rnh1 rnh201* strain is more comparable to the phenotype of

Figure 1. RNase H Activity Is Required for Efficient DSB Repair

(A) *rnh1 rnh201* cells are hypersensitive to DNA damage. Wild-type (WT) and mutant *S. pombe* strains were exposed to the indicated mutagens. CPT, camptothecin; HU, hydroxyurea; MMS, methyl methanesulfonate; UV, UV light; YEA, yeast extract adenine.

(B) Schematic demonstrating the I-PpoI cleavage sites (red lines) within the three chromosomes of the *S. pombe* genome. Cleavage sites at *chr III* represent the endogenous cleavage sites located within the rDNA repeats (~150 repeats). The location of the artificially integrated cleavage site (CS) and the *Hph* marker gene at *chr II* is shown.

(C) I-PpoI cleavage efficiency is similar in all I-PpoI-expressing strains. PCR amplification was performed on genomic DNA from the indicated strains before (OFF) and after (ON) a 2-hr I-PpoI induction, using primers spanning the cleavage site at *chr II* (PCR over CS) and primers in the *his3* locus as a control (PCR uncut *his3*). See Figure S1B for additional mutant strains.

(D) Double deletion of *rnh1* and *rnh201* or overexpression of Rnh1 leads to impaired survival following I-PpoI-induced DSBs. I-PpoI expression was induced for 2 hr, and cells were plated under non-I-PpoI-inducing conditions. Surviving colonies were counted after 2 days (black bars) and 4 days (gray bars). For the P*nmt1*-Rnh1 strain, overexpression of Rnh1 is indicated (+). Data are represented as mean + SEM of at least three biological replicates. The p values were obtained using the two-tailed unpaired Student's t test (**p 0.01; ****p 0.0001).

(E and F) Cleavage and recovery of the I-PpoI cleavage site at *chr II* (E) and at the ribosomal repeats at *chr III* (F). qPCR data are presented as relative qPCR signal compared to the non-cleaved sample (pre-I-PpoI induction) in the indicated strains. I-PpoI was induced for 2 hr, I-PpoI induction was stopped by the removal of anhydrotetracycline (ahTET) (time, t, = 0 hr), and the repair efficiency was measured at the indicated time points. Data are represented as mean SEM of three biological replicates.

See also Figures S1B, S1D, and S2A.

a mutant with impaired DSB repair, such as the *rad52* strain (Figure 1A).

Cells lacking RNase H activity accumulate RNA-DNA hybrids and R-loop structures genome-wide, which might influence the chromatin structure and/or the accessibility of the DNA to genotoxic chemicals. We wondered whether the strong DNA-damage sensitivity of the *rnh1 rnh201* mutant was due to either the increased level of DNA damage in response to DSB-inducing chemicals or the impairment of DNA repair in this mutant. In order to distinguish between these possibilities, we generated a tetracycline-inducible site-specific DSB system using the homing endonuclease I-PpoI (Figure S1A). *S. pombe* has one I-PpoI cleavage site within the rDNA, but since the rDNA is repeated ~150 times (separated in two clusters at both ends of *chr III*), I-PpoI has about 150 endogenous cleavage sites in the fission yeast genome. In addition to the natural cleavage sites, we integrated a single artificial cleavage site at *chr II* (Figure 1B). We induced I-PpoI expression for 2 hr in wild-type (WT), *rad52* , *rad51* , *pku80* , *rnh1* , *rnh201* , and *rnh1 rnh201* strains before plating the cells on media in which I-PpoI expression was repressed. The expression level and cleavage efficiency of I-PpoI, and the turnover dynamics of the protein following repression of I-PpoI transcription, were identical in all strains (Figures 1C, S1B, and S1D). Following I-PpoI-induced DSBs, ~73 of the WT cells were able to recover, while an identical strain lacking the I-PpoI open reading frame (ORF) (*no I-PpoI* strain) showed full (~100) recovery. Deletion of *Pku80* (*S. pombe* KU80 homolog), an essential component of the NHEJ repair pathway, did not influence the survival rate after chemical- (Figure 1A) or endonuclease-induced DSBs (76 , Figures 1D and S2A), indicating that the NHEJ pathway is dispensable for the DSB repair process in *S. pombe*. However, deletion of *Rad52* or *Rad51*, two essential factors in the HR-mediated repair pathway, drastically reduced the recovery rate after I-PpoI-induced DSBs to ~2 and ~14 , respectively. Interestingly, while *rnh1* or *rnh201* single deletions were indistinguishable from the WT, the *rnh1 rnh201* double-deletion strain could not recover after I-PpoI-induced DSBs (~10 recovery rate). Since the cleavage efficiency of I-PpoI was equivalent in all strains, this result suggests that RNase H activity is required for efficient HR-mediated DSB repair in *S. pombe*.

To monitor the DNA repair efficiency at the cleavage sites, we isolated the genomic DNA from the WT and mutant strains and quantified the repaired DNA strands by qPCR using primers spanning the cleavage sites (Figures 1E and S2A). We observed ~75 cleavage efficiency at the artificial cleavage site at *chr II* in all strains after 2-hr induction of the I-PpoI system. While WT and *pku80* mutant cells showed swift DSB repair, the DNA repair mutant *rad52* and the *rnh1 rnh201* mutants were unable to repair the I-PpoI-induced DSB. Similar results were observed at the cleavage sites at the repetitive rDNA loci (Figure 1F). Overall, using the site-specific I-PpoI system, we demonstrated that the strong DSB sensitivity of the *rnh1 rnh201* mutant was caused by a severely impaired DNA repair process and was not the result of increased DNA damage. Taken together, these results demonstrate that RNase H activity is necessary for efficient HR-mediated DSB repair in *S. pombe*.

Overexpression of Rnh1 Delays DSB Repair

The strong requirement for RNase H activity in the HR-mediated repair pathway suggests the presence of RNA-DNA hybrids during the course of DNA repair and indicates that these hybrids inhibit the completion of the repair process. We wondered whether these RNA-DNA hybrids are a by-product of the DNA repair process and act only as inhibitory structures or whether they are intermediate structures with an unknown function in the HR-mediated DNA repair. In order to answer this question, we studied the effect of Rnh1 overexpression in the DSB repair process. We used the strong, inducible Nmt1 promoter to overexpress the Rnh1 ORF in our I-PpoI DSB system (P*nmt1*-Rnh1) and monitored the DSB repair efficiency under Nmt1-inducing and non-inducing conditions. While Rnh1 overexpression did not affect the growth of *S. pombe* under normal growth conditions, it reduced the recovery rate after I-PpoI-induced DSBs to about ~3 . As per our standard recovery assay, we incubated the plates for 2 days at 30°C and counted the colonies to determine the recovery rate. Interestingly, we noticed that, if we kept these plates at 30°C for a longer period of time, additional small colonies appeared, and after 4 days of incubation, the recovery rate increased to ~17 in the P*nmt*1-Rnh1 strain (Figure 1D). This was only observed when both Rnh1 overexpression and I-PpoI cleavage were induced. The colony numbers and the corresponding recovery rates were unchanged in all other strains after an extended incubation time.

We also monitored the amount of repaired DNA strands directly at the I-PpoI cleavage sites. At *chr II*, we observed a strong delay in the repair process under conditions of Rnh1 overexpression, while at the ribosomal repeats, we could not detect any progression of the repair process during the 12-hr recovery period (Figures 1E and 1F). Overall, these results show that Rnh1 overexpression negatively influences DSB repair efficiency and suggest that RNA-DNA hybrids might represent a functional intermediate in the course of the HR-mediated repair process. To exclude the possibility that deletion or overexpression of RNase H could indirectly affect DNA repair by influencing the RNA levels of key DNA repair genes, we carried out genome-wide expression profiling in the *rnh1 rnh210* and P*nmt1*-Rnh1 strains. The results show that only a small number of genes are affected by deletion or overexpression of RNase H (Table S3), and none of these have any known function in the DNA repair process.

RNA-DNA Hybrids Accumulate at DSB Sites

In order to demonstrate direct evidence for the presence of RNA-DNA hybrids around the I-PpoI cleavage site, we carried out chromatin immunoprecipitation (ChIP) experiments using the S9.6 monoclonal antibody that specifically recognizes RNA-DNA hybrids of different lengths. We tested the presence of RNA-DNA hybrids 700 bp upstream of the I-PpoI cleavage site at *chr II*, either before or after 2-hr I-PpoI endonuclease induction (Figure 2A). We could not detect RNA-DNA hybrids at levels above background (no antibody control) in the absence of I-PpoI expression in the tested strains. However, after I-PpoI-induced DSBs, RNA-DNA hybrids were strongly enriched around the cleavage site in all tested strains. The amount of RNA-DNA hybrids was approximately the same in the WT,

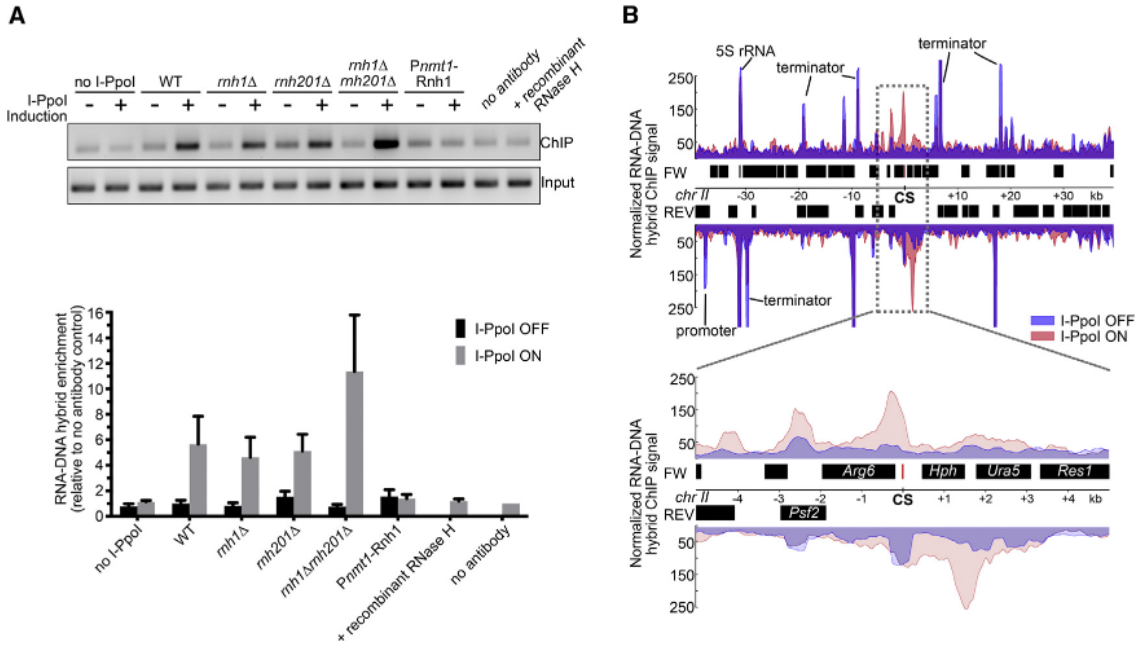

Figure 2. RNA-DNA Hybrids Accumulate around I-PpoI-Induced DSB Sites

(A) ChIP was performed in the indicated strains using the RNA-DNA hybrid-specific antibody S9.6 with (+) or without (-) 2-hr I-PpoI induction. The no-antibody control and the control using recombinant RNase H during the ChIP experiment were performed in the *rnh1 rnh201* strain with I-PpoI induction. The top panel shows an agarose gel of the PCR products of the ChIP and the input samples. The lower panel shows the relative enrichment of RNA-DNA hybrids in the indicated strains with (gray bars) or without (black bars) I-PpoI induction. For each strain, PCR products were quantified, and relative enrichment was calculated as ChIP/input relative to no-antibody control/input. Data are represented as mean + SEM of three biological replicates. See Figure S2B for cleavage efficiency data.

(B) ChIP-exo results for the *rnh1 rnh210* strain with (pink) or without (purple) 2-hr I-PpoI induction at the locus spanning the cleavage site (CS) at *chr II*, using the RNA-DNA hybrid-specific antibody S9.6. The upper and lower parts of the graphs represent the normalized ChIP-exo signal on the forward (FW) and reverse (REV) strands, respectively. The lower panel is a magnified view of the dotted box on the upper panel.

See also Figure S2B.

rnh1 , or *rnh201* strains, while the *rnh1 rnh201* strain showed significantly increased enrichment of the hybrids upon I-PpoI expression. In contrast, overexpression of Rnh1 (P*nmt1*-Rnh1 strain) led to the reverse effect and completely diminished the enrichment of the I-PpoI-induced RNA-DNA hybrids. Treatment of the cell extracts with recombinant bacterial RNase H during the ChIP protocol also decreased the signal to the background level, further validating the specificity of the ChIP signal. Overall, these experiments demonstrate that RNA-DNA hybrids form around DSBs and that extending or reducing the lifetime of these RNA-DNA hybrid structures (by depleting or overexpressing RNase H activity in the cells) can adversely affect the efficient completion of the repair process.

To more precisely determine the extent and directionality of the RNA-DNA hybrids around the DSB site, we used a modified ChIP-exo method to map RNA-DNA hybrids in the *rnh1 rnh210* strain (Figure 2B). This technique allows the strand-specific detection of RNA-DNA hybrids genome-wide, although with decreased sensitivity (the presence of RNA-DNA hybrids impairs the ligation efficiency during the library preparation). Overall, our data showed a similar genome-wide enrichment profile for RNA-DNA hybrids, as previously reported (Chan et al., 2014; El Hage et al., 2014); however, these hybrids were not affected by the induction or repression of I-PpoI expression. Examination of the region around the I-PpoI cleavage site at *chr II* upon I-PpoI induction revealed a strong increase in the amount of RNA-DNA hybrid structures up to 2 kb upstream and downstream of the cleavage site. With the exception of this region, the signal was highly similar between induced and non-induced samples. We could not reliably map the I-PpoI-induced RNA-DNA hybrids at the rDNA repeats due to the high background signal and/or the high basal level of RNA-DNA hybrids at this region. The distribution of the hybrids was strand specific, detected mainly on the forward DNA strand upstream of the cleavage site and on the reverse DNA strand downstream of the cleavage site. This distribution corresponds to RNA strands pointing away from the DSB site with their 3 ends, indicating RNA polymerase activity that transcribes away from the DSB in both directions. This topology is consistent with the possibility that the known HR-mediated repair intermediate structure, comprising 3 ssDNA tails around the DSB, is used as the template strand for Pol II transcription.

Pol II Is Recruited to DSB Sites

The formation of RNA-DNA hybrids around the DSB site suggests active transcription in this region, either before or after the DNA damage. One possibility is that transcripts that existed before the DSBs can hybridize with the ssDNA intermediates of the HR-mediated repair and form stable RNA-DNA hybrids

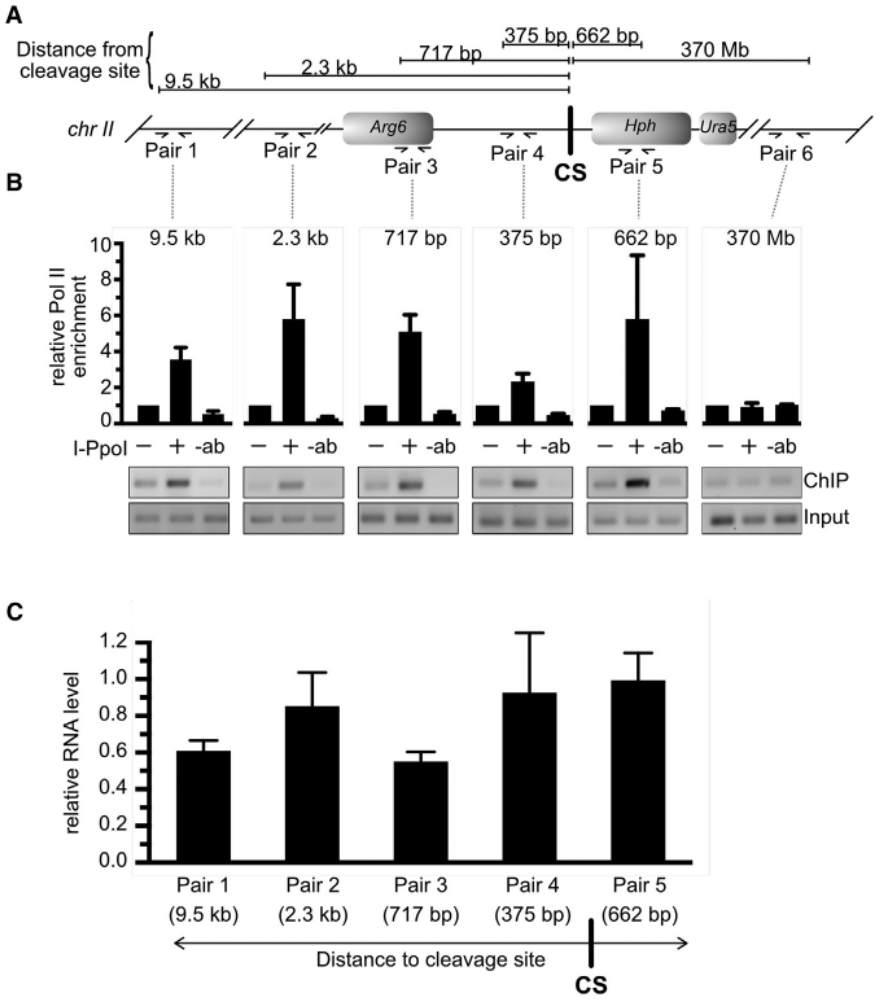

Figure 3. Pol II Is Recruited to I-PpoI-Induced DSB Sites

(A) Schematic indicating the locations and distance from the I-PpoI cleavage site (CS) of PCR primer pairs used in the Pol II ChIP experiments (not drawn to scale). Primer pair 6 amplifies a control region 370 Mb away from the cleavage site.

(B) ChIP was performed in the WT strain using anti-Pol II antibody (8WG16) with (+) or without (-) a 1-hr I-PpoI induction. The lower panel shows agarose gels of ChIP and input sample PCR products. The upper panel shows the relative enrichment of Pol II, where PCR products were quantified, and relative enrichment was calculated as ChIP/input relative to the no-I-PpoI-induction control. Data are represented as mean + SEM of three biological replicates.

(C) qRT-PCR results did not show increased RNA levels around the I-PpoI cleavage site at *chr II*. RNA was isolated before and after a 2-hr I-PpoI induction, and qPCR was performed with the indicated primer pairs. For each primer pair, RNA levels were determined relative to the non-I-PpoI-induced sample. Data are represented as mean + SEM of three biological replicates.

See also Figure S2B.

around the cleavage site. Alternatively, transcription around the DSB might be induced by the DSB itself, and the resulting nascent transcripts could form hybrids with their template strand. We carried out Pol II ChIP experiments using a non-phospho-specific antibody (8WG16) and monitored Pol II enrichment at three different locations in the vicinity of the I-PpoI cleavage site and at three locations further from the cleavage site (2 kb, 10 kb, and 370 Mb from the cleavage site; Figure 3A). Induction of I-PpoI led to a surge in the Pol II levels at all investigated locations around the DSB, including at the 2-kb and 10-kb distant sites; however, Pol II enrichment was not changed at the 370-Mb distant site (Figure 3B). These results demonstrate a rapid, DSB-dependent recruitment of Pol II to the I-PpoI cleavage site.

The strong increase in the Pol II levels around the site of the DSB prompted us to quantify potential changes in the transcript levels in this region. We isolated RNA from these cells, and after reverse transcription using random hexamers, we quantified the amount of cDNA by qPCR (Figure 3C). Interestingly, despite the strong increase in the Pol II levels, we could not detect increased RNA levels in this region. These results are consistent with the possibility that HR-mediated repair rapidly induces Pol II transcription around the DSB, but the resulting transcripts instantly hybridize with their template DNA strand and remain trapped in RNA-DNA hybrid structures. Considering that 3 ssDNA overhangs are created around the DSBs during HR-mediated repair, these intermediate ssDNA structures could serve as a template for Pol II transcription and would be naturally predisposed to hybridizing with the nascent RNA strand.

RPA Recruitment to DSBs Is Inhibited in the *rnh1 rnh201* Cells

In HR-mediated repair, the 5 DNA strands are digested by exonuclease activities (strand resection), leading to long 3 ssDNA overhangs around the DSB. The resulting ssDNA is then bound and protected by the heterotrimeric RPA complex, which is also essential for various signaling steps and for further progression of the repair process. To investigate whether RNA-DNA hybrids might affect the recruitment of RPA to the ssDNA overhangs, we monitored the enrichment of the RPA complex subunit Ssb2 around the DSB—before (0 hr) and at 2, 4, and 6 hr after I-PpoI induction—using ChIP (Figures 4A and 4B). We determined RPA enrichment at a distance of 2 kb and at 10 kb from the I-PpoI cleavage site in WT, *rnh1 rnh201* , and P*nmt1*-Rnh1 strains. Remarkably, we detected a strong decrease in the recruitment of RPA in the *rnh1 rnh201* strain compared to WT. Interestingly, overexpression of Rnh1 had the opposite effect, leading to a slightly increased RPA

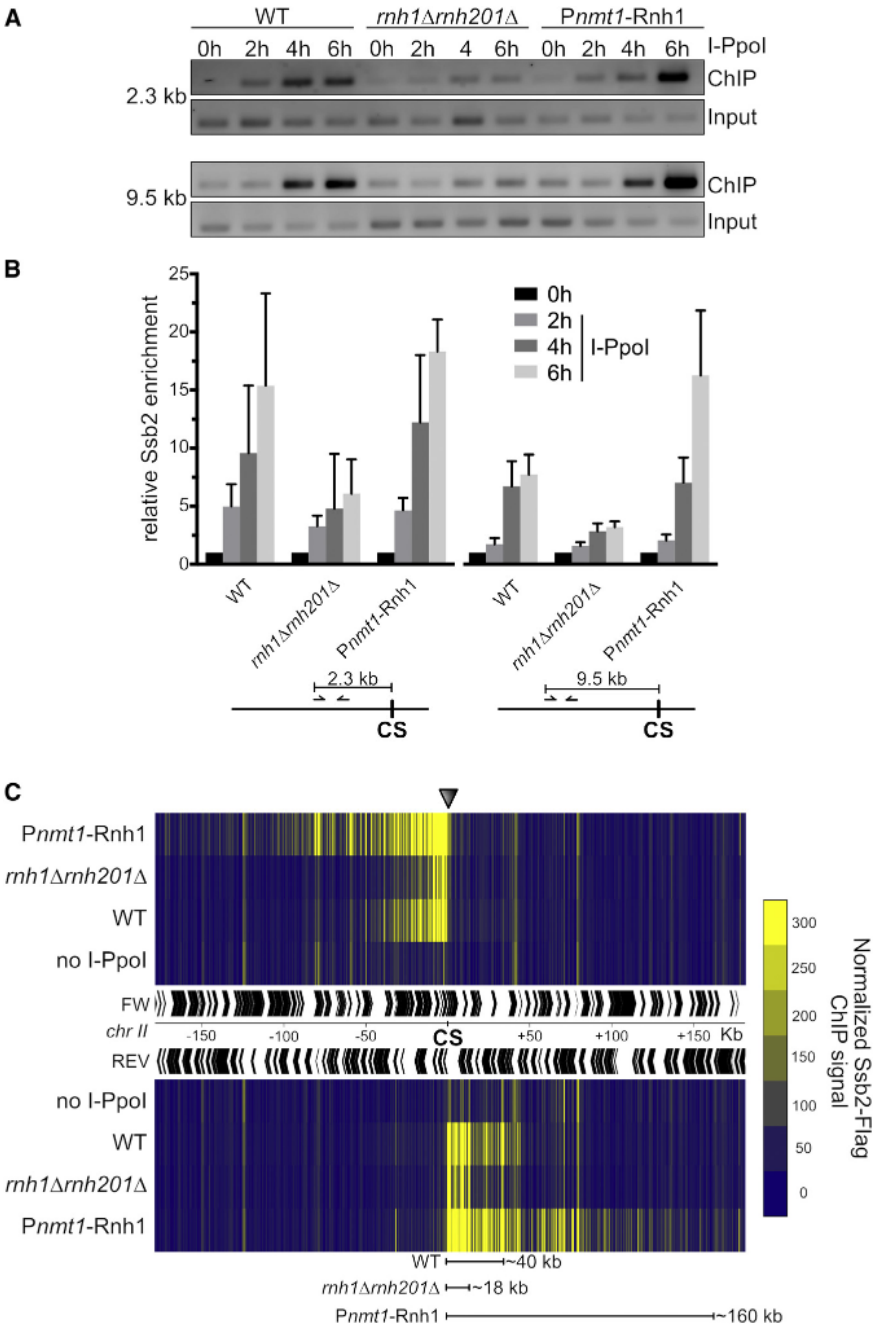

Figure 4. RPA Complex Recruitment around the DSB Site Is Impaired in *rnh1 rnh2 1* Cells

(A) ChIP was performed in the indicated strains, using the Ssb2-FLAG-tagged protein as bait. I-PpoI was uninduced (0 hr) or induced for 2, 4, or 6 hr. The agarose gels show the PCR products of ChIP and input samples using primer pairs binding at distances of 2.3 kb (upper) and 9.5 kb (lower) from the I-PpoI cleavage site at *chr II*. See also Figures S2C and S2D for cleavage efficiency controls.

(B) PCR products from the Ssb2-FLAG ChIP experiments were quantified, and relative enrichment was calculated as ChIP/input relative to the no-I-PpoI-induction control (0 hr) of the corresponding strain. Data are represented as mean + SEM of three biological replicates. CS, cleavage site.

(C) Heatmap showing the ChIP-exo results for Ssb2-Flag after a 4-hr I-PpoI induction in the indicated strains. The region of *chr II* around the I-PpoI cleavage site (CS) is shown. The upper and lower panels of the heatmap represent the ChIP-exo signal on the forward (FW) and reverse (REV) strands, respectively. Genes are indicated along the central axis by black arrows. The approximate distances of spread of Ssb2-Flag signal from the CS detected in the different strains are indicated on the figure.

See also Figures S2C and S2D.

enrichment at a distance of 2 kb from the DSB, while at a distance of 10 kb, the enrichment of RPA was significantly increased compared to WT.

Taken together, these results show that stabilized RNA-DNA hybrids around the DSB strongly interfere with the efficient recruitment of RPA to the ssDNA in *rnh1 rnh201* cells, thereby blocking the progression of HR-mediated DNA repair. Overexpression of RNase H1 shows the opposite effect and leads to increased RPA levels around the DSB, especially at the more distant (10-kb) location. This increase might reflect an extended ssDNA formation around the DSB in the Rnh1 overexpression strain. Alternatively, it might also indicate an arrest in the repair process after the RPA recruitment step, thereby prolonging the lifetime of the RPA-covered ssDNA intermediates.

To further investigate the length of the RPA-covered ssDNA fragments, we performed ChIP-exo experiments after the 4-hr induction of I-PpoI (Figure 4C). We observed an asymmetric localization of RPA around the I-PpoI cleavage site, showing strong enrichment on the forward strand upstream, and on the reverse strand downstream, of the cleavage site. This pattern is consistent with the predicted RPA binding of the 3 ssDNA fragments around the DSB. In WT cells, RPA enrichment of the ssDNA was detectable in a segment spanning ~40 kb upstream and downstream of the I-PpoI-induced DSB. Interestingly, the length of the RPA-bound ssDNA fragments were significantly shorter in the *rnh1 rnh201* strain, spreading less than a 20-kb distance from the DSB site. Overexpression of Rnh1 (P*nmt1*-Rnh1 strain) had the opposite effect, reaching up to a 160-kb distance upstream and downstream of the cleavage site. This surprising result indicates that, at least in a part of the population of the P*nmt1*-Rnh1 strain, the strand resection process could lead to an ssDNA formation spanning up to 300 kb, which is about 10 of an entire chromosome in *S. pombe*.

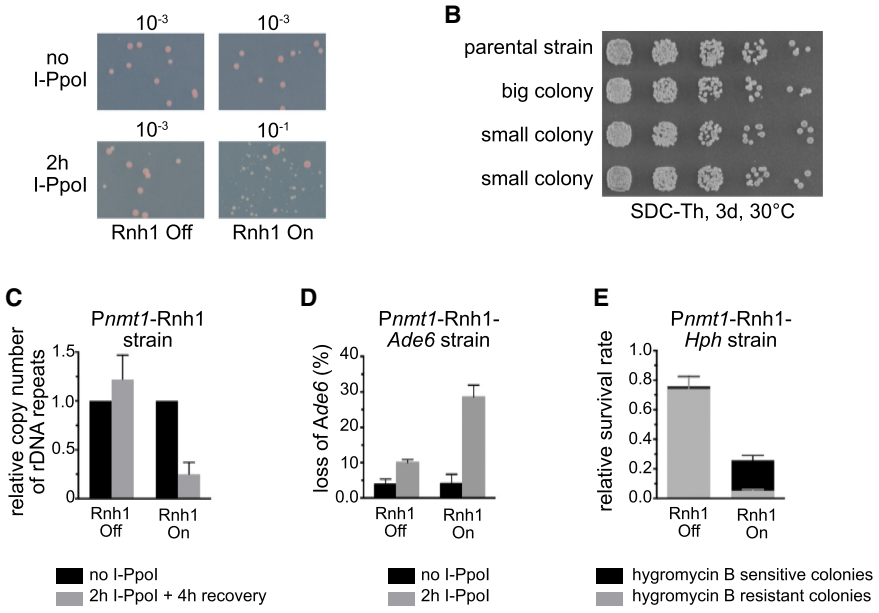

Figure 5. Overexpression of Rnh1 Leads to the Loss of Repeat Regions around DSBs

(A) Representative image of P*nmt1*-Rnh1 colony growth I-PpoI induction and Rnh1 overexpression. I-PpoI induction was performed for 2 hr prior to plating under non-inducing conditions, while Rnh1 overexpression was continuous for the duration of the experiment. Colonies were grown for 4 days at 30°C. Plating dilutions are indicated.

(B) 5-fold serial dilutions of cultures on SDC-Th medium (Rnh1 overexpression on), derived from representative small and big colonies of the P*nmt1*-Rnh1 strain with Rnh1 overexpression after I-PpoI induction and recovery. In the parental strain control, I-PpoI was not induced.

(C) Reduction of rDNA copy number under Rnh1 overexpression conditions after I-PpoI induction and recovery. Genomic DNA was isolated from P*nmt1*-Rnh1 strain Rnh1 overexpression and 2-hr I-PpoI induction and 4-hr recovery. rDNA repeats were quantified by qPCR. Data are presented as relative rDNA copy number in the I-PpoI-induced strain, compared to the non-induced strain, as mean + SEM of three biological replicates.

(D) Loss of *Ade6* marker gene after I-PpoI induction. *Ade6* was integrated in the rDNA repeat region (approximately five copies), and the strain was subjected to the indicated conditions. The percentage of colonies losing the *Ade6* marker genes was determined by replica plating the colonies onto SDC-Ade media. Data are represented as mean + SEM of five biological replicates.

(E) Repeat regions are lost around DSBs under conditions of Rnh1 overexpression. The P*nmt1*-Rnh1-*Hph* strain, with or without a 2-hr I-PpoI induction and with or without continuous Rnh1 overexpression, was plated under non-I-PpoI-inducing conditions. Surviving colonies were counted after 4 days, and loss of the *Hph* marker gene was determined by replica plating the colonies onto hygromycin B-containing media. Colonies with (hygromycin B resistant, indicated with gray bars) or without (hygromycin B sensitive, indicated with black bars) the *Hph* gene are represented in the stacked columns as mean + SEM of three biological replicates. See also Figure S2F.

RNase H1 Overexpression upon DSB Repair Leads to Loss of Repeat Regions

To further understand the effect of RNase H1 overexpression on HR-mediated DSB repair, we focused on the small colonies that appeared in the P*nmt1*-Rnh1 strain after DNA damage. These tiny colonies were observed only after I-PpoI-induced DSBs and only if Rnh1 was overexpressed (Figure 5A). Intriguingly, when we tried to isolate these small colonies, they did not keep their slow-growing phenotype, but they were able to recover to normal growth behavior (Figure 5B). Since the natural cleavage site of I-PpoI is in the rDNA, we wondered whether the original slow-growth phenotype could be attributed to the extensive loss of ribosomal repeats in these cells. It is known that ribosomal repeats use a specific gene amplification system to restore their copy number if it falls below a critical volume, which could explain the growth rate recovery after a number of cell divisions (Kobayashi, 2014). To investigate this possibility, we induced I-PpoI-mediated DSBs for 2 hr in the P*nmt1*-Rnh1 strains with or without Rnh1 overexpressing conditions, and after a 4-hr recovery, we isolated genomic DNA and quantified the average number of rDNA repeats in the cell population by qPCR (Figure 5C). We used a primer pair homologous to the intergenic spacer region, 3.8 kb from the I-PpoI cleavage site, and the results were normalized to the rDNA copy number before I-PpoI induction. Under RNase H1 overexpression conditions, we observed a dramatic loss of rDNA repeats after I-PpoI-induced DSBs. In strong contrast, the rDNA repeat copy number was slightly increased in the non-overexpressing conditions after I-PpoI induction. To confirm these results, we integrated an *Ade6* marker gene into the rDNA repeat region of the P*nmt1*-Rnh1 strain (referred to as P*nmt1*-Rnh1-*Ade6*) and monitored the loss of the *Ade6* gene after 2 hr of I-PpoI induction followed by 4 days of recovery (Figure 5D). Due to the highly repetitive nature of the rDNA locus, the *Ade6* gene integrated into multiple repeats (approximately five copies). We could detect the loss of the *Ade6* marker only if all of its copies were lost. However, this system has the advantage that, once all the *Ade6* genes are lost, the cells cannott re-amplify them, in contrast to the ribosomal repeats. When Rnh1 overexpression was repressed (Rnh1 OFF), only ~10 of the surviving cells showed the ade- phenotype, indicating a moderate rDNA repeat loss under these conditions. However, if Rnh1 overexpression was induced (Rnh1 ON), 30 of the surviving cells lost all copies of the *Ade6* gene, confirming the significantly higher degree of rDNA repeat loss under these conditions. Overall, these results confirmed that overexpression of RNase H1 leads to a strong loss of rDNA repeats during DSB repair, which is likely also the cause of the very slow growth rate of these cells before they can re-amplify their rDNA repeats.

To extend this observation beyond the rDNA locus, we modified the I-PpoI cleavage site at *chr II* in our P*nmt1*-Rnh1 strain by integrating 500-bp-long repeat regions upstream and downstream of the I-PpoI cleavage site. These repeats were separated by an ~5-kb unique DNA sequence, which included

the cleavage site for I-PpoI and the hygromycin phosphotransferase (*Hph*) gene, providing resistance against hygromycin B. This strain will be referred to as the P*nmt1*-Rnh1-*Hph* strain (Figure S2E). We induced I-PpoI expression for 2 hr in the presence (Rnh1 overexpression OFF) or absence (Rnh1 overexpression ON) of thiamine, and after 4 days of recovery at 30°C, the colonies were replica plated to hygromycin B-containing media (Figure 5E). Remarkably, ~80 of the recovered colonies lost their *Hph* marker gene under conditions of Rnh1 overexpression, while only ~2 of the colonies were hygromycin B sensitive if the Rnh1 overexpression was turned off. We sequenced the region around the I-PpoI cleavage site at *chr II* from ten hygromycin B-sensitive colonies and confirmed the seamless loss of one of the repeats and the entire region between the repeats, indicating an intrachromosomal recombination between the two repeats. This corresponds to a 40-fold increase in the frequency of intrachromosomal recombination under conditions of Rnh1 overexpression. Taken together, these results show that overexpression of RNase H1 leads to the loss of repeat regions around DSBs, both at the rDNA locus and at other genomic regions with direct DNA repeats.

To exclude the possibility that the inhibitory effects of RNase H deletions or overexpression on the DSB repair process are specific to the repetitive rDNA locus, we set up an inducible DSB system using the SmaI endonuclease, which does not generate DSBs at the rDNA region. SmaI has 208 restriction sites distributed throughout the fission yeast genome; however, none of these sites are located in the rDNA locus or at other repetitive loci. While ~77 of the WT cells recovered following SmaI-induced DSBs, survival in the *rnh1 rnh201* double-deletion strain was reduced to ~10 (Figure S2G). This confirms the results of the I-PpoI system and demonstrates that the requirement of RNase H activity in the DSB repair process is independent of any effect of the rDNA locus. However, overexpression of RNase H1 in the SmaI-induced DSB system had a less severe effect on survival rate (~41) compared to the I-PpoI system (~17), which is consistent with our finding that the deleterious effect of Rnh1 overexpression upon I-PpoI-induced DSBs can be partly attributed to the severe loss of rDNA repeats. Since the SmaI enzyme does not induce DSBs at the rDNA locus, the adverse effects of the rDNA repeat loss cannot be observed in this system. Accordingly, the small colonies representing the recovering cells after severe rDNA repeat loss in the I-PpoI system upon RNase H1 overexpression were not observed in the SmaI-induced DSB system. These observations strongly suggest that the DSB-induced RNA-DNA hybrids have a protective function against unwanted intrachromosomal recombination between repeat regions during HR-mediated repair and that reducing the lifetime of these hybrids by overexpressing RNase H1 can result in the loss of the genetic information around the DSB site. Since the eukaryotic genome is full of repeat regions, the protective function of the RNA-DNA hybrids upon DSB repair might be essential for the correct maintenance of the genome.

DISCUSSION

RNase H enzymes are evolutionarily conserved from prokaryotes to humans and are present in nearly all living organisms. Their suggested physiological functions range from degrading Okazaki fragments during replication and removing mis-incorporated ribonucleotides from the DNA duplex to degrading transcription-associated R-loops. Surprisingly, RNase H activity is not essential for the survival of yeast cells, and deletion of both RNase H genes does not cause an obvious phenotype under normal growth conditions. This can be partially explained by the fact that most of the suggested in vivo functions of RNase H enzymes can be carried out by other enzymes or complexes, such as Okazaki-fragment degradation by Fen1/Dna2/Exo1 (Dalgaard, 2012), the removal of single mis-incorporated ribonucleotides from the genome by Top1 and the base excision repair machinery (Williams et al., 2013), and the elimination of R-loop structures by the helicase sentaxin (yeast Sen1) (Skourti-Stathaki et al., 2011). Our study has revealed a physiological function, undetected until now, for RNase H enzymes and has shown that RNase H activity is essential for the HR-mediated DSB-repair process in *S. pombe*. Both the DSB-repair machinery and RNase H genes are highly conserved during evolution, suggesting that the involvement of RNA-DNA hybrids and RNase H activity in DNA repair might be a general mechanism throughout evolution. Indeed, in the evolutionarily highly distant *S. cerevisiae*, deletion of RNase H genes leads to a strong sensitivity against DNA-damaging chemicals, similar to what we observed in *S. pombe* (Arudchandran et al., 2000; Lazzaro et al., 2012).

During the process of HR-mediated DSB repair, the 5 DNA strands are exonucleotically degraded to generate long, single-stranded 3 DNA ends. These ssDNA regions are stabilized by the ssDNA-binding RPA complex, which is subsequently replaced by the Rad51 recombinase to catalyze homology search and strand invasion to the sister chromatid. Our study showed that Pol II is also recruited to these ssDNA regions and that it promotes the formation of RNA-DNA hybrids (Figure 6). Previous publications reported Pol II transcriptional arrest around DSBs, seemingly contradicting our results. However, Pol II arrest is mediated by the DNA protein kinase (DNAPK) (Pankotai et al., 2012), which is only active during NHEJ repair and which does not interfere with Pol II transcription during HR-mediated repair. Since there are no sequence-specific DNA elements around DSBs, what is the signal for transcription initiation for Pol II in these regions? Remarkably, the addition of a short ssDNA segment with a 3 -OH terminus to a double-stranded DNA (dsDNA) produces a highly efficient template for Pol II transcription in vitro (Kadesch and Chamberlin, 1982). This technique is widely used to study transcription elongation and termination using purified RNA polymerase core complex, without the addition of factors necessary for transcription initiation. Interestingly, these ssDNA-tailed templates are also excellent templates for the transcription of RNA polymerases I and III (Pol I and Pol III, respectively), without the addition of sequence-specific elements. During HR-mediated DSB repair, the ssDNA segments, generated by the 5 end resection process, might also serve as highly efficient, sequence-independent transcription initiation sites. RNA polymerases might be among the first factors that can detect ssDNA fragments in vivo and jump-start transcription without the requirement of the assembly of the large preinitiation complex (PIC) and the recruitment of additional regulatory proteins. This elongating Pol II complex could follow the

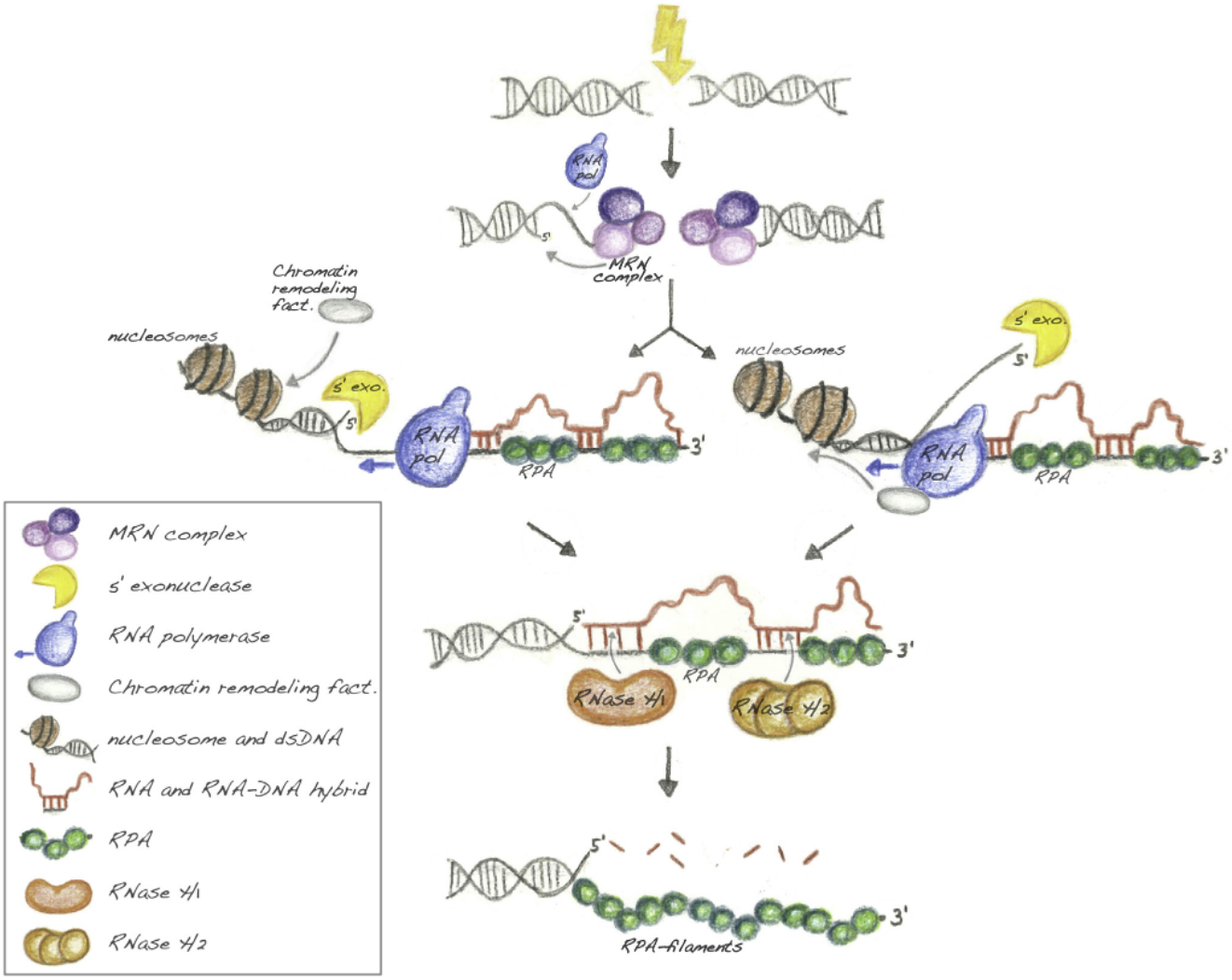

Figure 6. RNA-DNA Hybrids and RNase H Activity Are Required for Efficient DSB Repair

Suggested model for the HR-mediated DSB repair pathway. Following the appearance of a DSB, the MRN complex is recruited to the broken DNA ends and, with the help of Sae2, initiates 5 end resection. Pol II is recruited to the 3 ssDNA overhangs and jump-starts transcription, without the requirement of PIC assembly or the recruitment of additional regulatory proteins. The nascent RNA transcripts are prone to re-hybridize with the ssDNA template strand and form RNA-DNA hybrids, which directly compete with the ssDNA-binding RPA complex. Subsequent, long-range resection of the 5 strand is performed by the 5 -3 exonuclease Exo1 or the Dna2-Sgs1/BLM complex. Additional chromatin remodeling activities likely facilitate the progression of nucleases through the chromatin environment. Pol II transcription either follows the strand resection process (left) or actively drives strand resection by opening the chromatin and the DNA helix ahead of the nucleases (right). RNA-DNA hybrids might play a role in controlling the speed and the length of the strand resection process by stalling or terminating Pol II transcription. RNA-DNA hybrids need to be degraded by RNase H enzymes in order to achieve full RPA loading on the ssDNA overhangs and to complete the DNA repair process.

exonucleases involved in the strand resection process and generate long ncRNAs from the ssDNA template. Since the non-template DNA strand is degraded, the nascent transcripts would be more prone to re-hybridize with their ssDNA template and form RNA-DNA hybrids, directly competing with the recruitment of the RPA complex. These RNA-DNA hybrids are eliminated by RNase H activity in order to achieve full RPA loading and to complete the DNA repair process. This model is consistent with the observed Pol II recruitment and detection of RNA-DNA hybrids around the DSB site. Furthermore, we showed that the recruitment of RPA to the ssDNA is strongly impaired in the *rnh1 rnh210* mutant in which RNA-DNA hybrids are stabilized.

An alternative possibility to the model whereby Pol II transcription passively follows the 5 -3 end resection is that Pol II transcription plays an active role in opening the chromatin and the DNA strands ahead of the exonucleases. It is known that the initial step of the end resection process is carried out by the MRN complex, leading to a short ssDNA segment (Mimitou and Symington, 2011). In a second step, a faster and more extensive resection occurs with the help of the 5 -3 exonuclease Exo1 or the Sgs1-Dna2 complex, creating long ssDNA regions

(tens of kilobases). However, the end resection occurs in the context of chromatin; therefore, access to the underlying DNA is restricted. A recent study in *S. cerevisiae* showed that efficient resection of Sgs1-Dna2 is dependent on nucleosome-free regions adjacent to the DSB site and that the resection by Exo1 is completely blocked by the presence of nucleosomes (Adkins et al., 2013). Although a large number of chromatin-remodeling enzymes were suggested to be involved in the HR-mediated DSB repair process—including RSC, SWI/SNF, INO80, SWR-C, and Fun30 (Eapen et al., 2012)—their exact functions and the recruitment mechanisms to the DSB sites remain obscure (House et al., 2014). We showed that Pol II transcription is initiated around the DSB site, probably as a result of the short ssDNA segments derived from the initial step of the end resection process by the MRN complex. Once the Pol II machinery is in elongation mode, it recruits chromatin remodelers and histone chaperones to open the chromatin ahead of the transcription bubble. The FACT complex has a key role in this process, and interestingly, various studies have also demonstrated that the FACT complex plays an important role in DSB repair (Keller and Lu, 2002; Heo et al., 2008; Oliveira et al., 2014). If Pol II transcription actively drives the strand resection process, the speed and length of the Pol II elongation would also influence the speed and length of the strand resection and, thereby, the length of the ssDNA regions involved in the homology search and strand exchange. Indeed, we can detect major differences in the length of the RPA-covered ssDNA segments when RNase H activity is deleted or overexpressed in the cell, but how does the stabilization or destabilization of RNA-DNA hybrids affect the elongating Pol II around the DSB sites? It is well established that the formation of RNA-DNA hybrids between the nascent RNA and the template DNA strand lead to Pol II stalling and, eventually, to transcription termination (Skourti-Stathaki et al., 2011, 2014; Zhao et al., 2016; Belotserkovskii et al., 2013). It was previously reported that transcription termination sites have high levels of RNA-DNA hybrids, and this was also confirmed by our RNA-DNA hybrid ChIP-exo results. Stabilization of RNA-DNA hybrids, by deleting both RNase H genes, could lead to frequent stalling and early termination of the elongating Pol II around the DSB sites and, subsequently, shorter ssDNA segment formation. In this model, destabilization of RNA-DNA hybrids by the overexpression of RNase H1 would have the opposite effect by increasing the speed and distance of Pol II transcription, resulting in excessive ssDNA formation. This is in agreement with our experimental data, which showed a decrease in the length of the RPA-covered ssDNA segments around the DSB in the *rnh1 rnh201* strain, while overexpression of Rnh1 led to extra-long ssDNA fragments. Excessive strand resection and the resulting extra-long ssDNA fragments can expose complementary sequences at direct repeats (such as the rDNA repeats) and lead to inaccurate template selection during the 3 end invasion step and the loss of the repeat sequences (Hastings et al., 2009). This mechanism could explain the observed loss of repeat regions around DSBs under conditions of RNase H1 overexpression. Although this model would be fully compatible with our results, our experimental setup did not allow the direct testing of the Pol II requirement in the HR-mediated repair process. Further studies are necessary to distinguish between these models and address whether Pol II transcription, indeed, plays an active role in the strand resection process.

Interestingly, several studies have reported a connection between RNA-DNA hybrids, RNase H, and the DNA repair machinery. In a recent study, a GFP-tagged, catalytically inactive form of RNase H1 was used to visualize RNA-DNA hybrids in human cells. Britton et al. (2014) used laser micro-irradiation to induce DSBs and showed the transient recruitment of the GFP signal to the induced DSBs, suggesting that, similar to our data in *S. pombe*, RNA-DNA hybrids also appear transiently at DSBs in higher eukaryotes. Furthermore, this recruitment was strictly dependent on transcription, since actinomycin D treatment abolished the appearance of RNA-DNA hybrids. These results are also in agreement with our data and provide further evidence for the involvement of active RNA polymerase transcription in the DSB repair process. Another interesting observation is that the *Escherichia coli* RNase H1 can directly interact with the ssDNA-binding protein (SSB), the *E. coli* ortholog of the eukaryotic RPA complex (Petzold et al., 2015), and this interaction stimulates the activity of RNase H1. A proteomic screen for RPA-binding proteins in human cells also identified RNase H1 as a binding partner, indicating that this interaction might be evolutionarily conserved (Maréchal et al., 2014). These results raise the possibility that the degradation of RNA-DNA hybrids at DSBs by RNase H enzymes might be actively regulated by the repair machinery. However, our study clearly demonstrates the formation of RNA-DNA hybrids during HR-mediated DSB repair and the requirement of RNase H enzymes to degrade these intermediate structures and allow the completion of the repair process. It will be important to extend this study to higher eukaryotes, as the findings presented here suggest that RNase H enzymes may provide potential new therapeutic targets for inhibiting efficient DSB repair.

STAR METHODS

Detailed methods are provided in the online version of this paper and include the following:

SUPPLEMENTAL INFORMATION

Supplemental Information includes two figures and three tables and can be found with this article online at http://dx.doi.org/10.1016/j.cell.2016.10.001.

AUTHOR CONTRIBUTIONS

C.O., R.T., I.S., and T.F. designed the experiments; C.O., R.T., G.S., and N.D. prepared reagents and strains; C.O., R.T., and G.S. performed the experiments; G.S. and T.F. analyzed high-throughput data; and C.O. and T.F. wrote the manuscript.

ACKNOWLEDGMENTS

We thank Jutta Worsch for her excellent technical assistance, Michael Brunner and Martin Kos for discussions and ideas, Emmalene Bartlett for proofreading the manuscript, Steven L. Sanders for providing various I-PpoI plasmids, and Adam Watson for the pAW-HO-DSR vector. This work was supported by grants from the Ministry of Science, Research and the Arts Baden-Wuerttemberg (to T.F.) and from the Deutsche Forschungsgemeinschaft Research Grants Programme FI 1790/2-1 (to T.F. and R.T.). N.D. was supported with scholarship (Funding ID: 57034101) from the German Academic Exchange Service (DAAD). I.S. and T.F. are investigators of the Cluster of Excellence: CellNetworks and acknowledges support through EcTop1 and EcTop5.

Received: April 14, 2016
Revised: August 16, 2016
Accepted: September 29, 2016
Published: October 27, 2016

REFERENCES

Adkins, N.L., Niu, H., Sung, P., and Peterson, C.L. (2013). Nucleosome dynamics regulates DNA processing. Nat. Struct. Mol. Biol. *20*, 836–842.

Aguilera, A., and García-Muse, T. (2012). R loops: from transcription byproducts to threats to genome stability. Mol. Cell *46*, 115–124.

Arudchandran, A., Cerritelli, S., Narimatsu, S., Itaya, M., Shin, D.Y., Shimada, Y., and Crouch, R.J. (2000). The absence of ribonuclease H1 or H2 alters the sensitivity of Saccharomyces cerevisiae to hydroxyurea, caffeine and ethyl methanesulphonate: implications for roles of RNases H in DNA replication and repair. Genes Cells *5*, 789–802.

Belotserkovskii, B.P., Neil, A.J., Saleh, S.S., Shin, J.H., Mirkin, S.M., and Hanawalt, P.C. (2013). Transcription blockage by homopurine DNA sequences: role of sequence composition and single-strand breaks. Nucleic Acids Res. *41*, 1817–1828.

Blackwood, J.K., Rzechorzek, N.J., Bray, S.M., Maman, J.D., Pellegrini, L., and Robinson, N.P. (2013). End-resection at DNA double-strand breaks in the three domains of life. Biochem. Soc. Trans. *41*, 314–320.

Britton, S., Dernoncourt, E., Delteil, C., Froment, C., Schiltz, O., Salles, B., Frit, P., and Calsou, P. (2014). DNA damage triggers SAF-A and RNA biogenesis factors exclusion from chromatin coupled to R-loops removal. Nucleic Acids Res. *42*, 9047–9062.

Cerritelli, S.M., and Crouch, R.J. (2009). Ribonuclease H: the enzymes in eukaryotes. FEBS J. *276*, 1494–1505.

Cerritelli, S.M., Frolova, E.G., Feng, C., Grinberg, A., Love, P.E., and Crouch, R.J. (2003). Failure to produce mitochondrial DNA results in embryonic lethality in Rnaseh1 null mice. Mol. Cell *11*, 807–815.

Chan, Y.A., Aristizabal, M.J., Lu, P.Y., Luo, Z., Hamza, A., Kobor, M.S., Stirling, P.C., and Hieter, P. (2014). Genome-wide profiling of yeast DNA:RNA hybrid prone sites with DRIP-chip. PLoS Genet. *10*, e1004288.

Chapman, J.R., Taylor, M.R., and Boulton, S.J. (2012). Playing the end game: DNA double-strand break repair pathway choice. Mol. Cell *47*, 497–510.

Chowdhury, D., Choi, Y.E., and Brault, M.E. (2013). Charity begins at home: non-coding RNA functions in DNA repair. Nat. Rev. Mol. Cell Biol. *14*, 181–189.

Crow, Y.J., Leitch, A., Hayward, B.E., Garner, A., Parmar, R., Griffith, E., Ali, M., Semple, C., Aicardi, J., Babul-Hirji, R., et al. (2006). Mutations in genes encoding ribonuclease H2 subunits cause Aicardi-Goutières syndrome and mimic congenital viral brain infection. Nat. Genet. *38*, 910–916.

Dalgaard, J.Z. (2012). Causes and consequences of ribonucleotide incorporation into nuclear DNA. Trends Genet. *28*, 592–597.

Eapen, V.V., Sugawara, N., Tsabar, M., Wu, W.H., and Haber, J.E. (2012). The Saccharomyces cerevisiae chromatin remodeler Fun30 regulates DNA end resection and checkpoint deactivation. Mol. Cell. Biol. *32*, 4727–4740.

El Hage, A., Webb, S., Kerr, A., and Tollervey, D. (2014). Genome-wide distribution of RNA-DNA hybrids identifies RNase H targets in tRNA genes, retrotransposons and mitochondria. PLoS Genet. *10*, e1004716.

Francia, S., Michelini, F., Saxena, A., Tang, D., de Hoon, M., Anelli, V., Mione, M., Carninci, P., and d'Adda di Fagagna, F. (2012). Site-specific DICER and DROSHA RNA products control the DNA-damage response. Nature *488*, 231–235.

Hastings, P.J., Lupski, J.R., Rosenberg, S.M., and Ira, G. (2009). Mechanisms of change in gene copy number. Nat. Rev. Genet. *10*, 551–564.

Helmrich, A., Ballarino, M., Nudler, E., and Tora, L. (2013). Transcription-replication encounters, consequences and genomic instability. Nat. Struct. Mol. Biol. *20*, 412–418.

Heo, K., Kim, H., Choi, S.H., Choi, J., Kim, K., Gu, J., Lieber, M.R., Yang, A.S., and An, W. (2008). FACT-mediated exchange of histone variant H2AX regulated by phosphorylation of H2AX and ADP-ribosylation of Spt16. Mol. Cell *30*, 86–97.

House, N.C.M., Koch, M.R., and Freudenreich, C.H. (2014). Chromatin modifications and DNA repair: beyond double-strand breaks. Front. Genet. *5*, 296.

Kadesch, T.R., and Chamberlin, M.J. (1982). Studies of in vitro transcription by calf thymus RNA polymerase II using a novel duplex DNA template. J. Biol. Chem. *257*, 5286–5295.

Keller, D.M., and Lu, H. (2002). p53 serine 392 phosphorylation increases after UV through induction of the assembly of the CK2.hSPT16.SSRP1 complex. J. Biol. Chem. *277*, 50206–50213.

Keskin, H., Shen, Y., Huang, F., Patel, M., Yang, T., Ashley, K., Mazin, A.V., and Storici, F. (2014). Transcript-RNA-templated DNA recombination and repair. Nature *515*, 436–439.

Kobayashi, T. (2014). Ribosomal RNA gene repeats, their stability and cellular senescence. Proc. Jpn. Acad. Ser. B, Phys. Biol. Sci. *90*, 119–129.

Langmead, B., and Salzberg, S.L. (2012). Fast gapped-read alignment with Bowtie 2. Nat Methods *9*, 357–359.

Lazzaro, F., Novarina, D., Amara, F., Watt, D.L., Stone, J.E., Costanzo, V., Burgers, P.M., Kunkel, T.A., Plevani, P., and Muzi-Falconi, M. (2012). RNase H and postreplication repair protect cells from ribonucleotides incorporated in DNA. Mol. Cell *45*, 99–110.

Lee, H.C., Chang, S.S., Choudhary, S., Aalto, A.P., Maiti, M., Bamford, D.H., and Liu, Y. (2009). qiRNA is a new type of small interfering RNA induced by DNA damage. Nature *459*, 274–277.

Li, H., Handsaker, B., Wysoker, A., Fennell, T., Ruan, J., Homer, N., Marth, G., Abecasis, G., and Durbin, R. (2009). The sequence alignment/map format and SAMtools. Bioinformatics *25*, 2078–2079.

Maréchal, A., Li, J.M., Ji, X.Y., Wu, C.S., Yazinski, S.A., Nguyen, H.D., Liu, S., Jiménez, A.E., Jin, J., and Zou, L. (2014). PRP19 transforms into a sensor of RPA-ssDNA after DNA damage and drives ATR activation via a ubiquitin-mediated circuitry. Mol. Cell *53*, 235–246.

Mimitou, E.P., and Symington, L.S. (2008). Sae2, Exo1 and Sgs1 collaborate in DNA double-strand break processing. Nature *455*, 770–774.

Mimitou, E.P., and Symington, L.S. (2009). Nucleases and helicases take center stage in homologous recombination. Trends Biochem. Sci. *34*, 264–272.

Mimitou, E.P., and Symington, L.S. (2011). DNA end resection–unraveling the tail. DNA Repair (Amst.) *10*, 344–348.

Ohsawa, R., Seol, J.H., and Tyler, J.K. (2013). At the intersection of non-coding transcription, DNA repair, chromatin structure, and cellular senescence. Front. Genet. *4*, 136.

Oliveira, D.V., Kato, A., Nakamura, K., Ikura, T., Okada, M., Kobayashi, J., Yanagihara, H., Saito, Y., Tauchi, H., and Komatsu, K. (2014). Histone chaperone FACT regulates homologous recombination by chromatin remodeling through interaction with RNF20. J. Cell Sci. *127*, 763–772.

Pankotai, T., Bonhomme, C., Chen, D., and Soutoglou, E. (2012). DNAPKcs-dependent arrest of RNA polymerase II transcription in the presence of DNA breaks. Nat. Struct. Mol. Biol. *19*, 276–282.

Petzold, C., Marceau, A.H., Miller, K.H., Marqusee, S., and Keck, J.L. (2015). Interaction with single-stranded DNA binding protein stimulates Escherichia coli ribonuclease HI enzymatic activity. J. Biol. Chem. *290*, 14626–14636.

Rhee, H.S., and Pugh, B.F. (2012). ChIP-exo method for identifying genomic location of DNA-binding proteins with near-single-nucleotide accuracy. Curr. Protoc. Mol. Biol., Chapter 21, Unit 21.24.

Skourti-Stathaki, K., Proudfoot, N.J., and Gromak, N. (2011). Human senataxin resolves RNA/DNA hybrids formed at transcriptional pause sites to promote Xrn2-dependent termination. Mol. Cell *42*, 794–805.

Skourti-Stathaki, K., Kamieniarz-Gdula, K., and Proudfoot, N.J. (2014). R-loops induce repressive chromatin marks over mammalian gene terminators. Nature *516*, 436–439.

Vijg, J., and Suh, Y. (2013). Genome instability and aging. Annu. Rev. Physiol. *75*, 645–668.

Wei, W., Ba, Z., Gao, M., Wu, Y., Ma, Y., Amiard, S., White, C.I., Rendtlew Danielsen, J.M., Yang, Y.-G., and Qi, Y. (2012). A role for small RNAs in DNA double-strand break repair. Cell *149*, 101–112.

Williams, J.S., Smith, D.J., Marjavaara, L., Lujan, S.A., Chabes, A., and Kunkel, T.A. (2013). Topoisomerase 1-mediated removal of ribonucleotides from nascent leading-strand DNA. Mol. Cell *49*, 1010–1015.

Zhao, D.Y., Gish, G., Braunschweig, U., Li, Y., Ni, Z., Schmitges, F.W., Zhong, G., Liu, K., Li, W., Moffat, J., et al. (2016). SMN and symmetric arginine dimethylation of RNA polymerase II C-terminal domain control termination. Nature *529*, 48–53.

Zhou, Y., Zhu, J., Schermann, G., Ohle, C., Bendrin, K., Sugioka-Sugiyama, R., Sugiyama, T., and Fischer, T. (2015). The fission yeast MTREC complex targets CUTs and unspliced pre-mRNAs to the nuclear exosome. Nat. Commun. *6*, 7050.

Zhu, Z., Chung, W.H., Shim, E.Y., Lee, S.E., and Ira, G. (2008). Sgs1 helicase and two nucleases Dna2 and Exo1 resect DNA double-strand break ends. Cell *134*, 981–994.

STAR METHODS

KEY RESOURCES TABLE

REAGENT or RESOURCE	SOURCE	IDENTIFIER
Antibodies		
S9.6 anti RNA-DNA hybrid	Kerafast	ENH001
RNA polymerase II (8WG16)	Thermo Fischer	MA1-26249
Anti-Flag M2 Pox monoclonal	Sigma Aldrich	A8592; RRID: AB_439702
Chemicals, Peptides, and Recombinant Proteins		
T4 DNA Polymerase	NEB	M0203L
T4 Polynucleotide Kinase	NEB	M0201L
Klenow Fragment (exo-)	NEB	M0212L
T4 DNA Ligase	NEB	M0202L
Lambda Exonuclease	NEB	M0262L
RecJf Exonuclease	NEB	M0264L
Phi29 DNA Polymerase	NEB	M0264L
Taq DNA Polymerase	Sigma Aldrich	D4545
Q5 DNA Polymerase	NEB	M0491L
FAST SYBR Green Master Mix	Applied Biosystems	4385612
Anhydrotetracycline-hydrocloride	Sigma Aldrich	37919
Ambion RNase Cocktail	Thermo Fischer	AM2286
Proteinase K	Thermo Fischer	AM2548
PMSF	Sigma Aldrich	78830
FY protease inhibitor cocktail	Serva	39104.01
Anti-Flag M2 affinity gel agarose beads	Sigma	A2220
PureProteome Protein G magnetic beads	Millipore	LSKNAGG10
PureProteome Protein A magnetic beads	Millipore	LSKNAGA10
Protein A Sepharose 4 Fast Flow	Sigma Aldrich	GE17-5280-01
Protein G Sepharose 4 Fast Flow	Sigma Aldrich	GE17-0618-01
Agencourt AMPure XP	Beckman-Coulter	A63881
Camptothecin	Sigma Aldrich	C9911
Methyl methanesulfonate	Sigma Aldrich	129925
Hydroxyurea	Sigma Aldrich	H8627
TURBO DNase	Thermo Fischer	AM2238
M-MLV reverse transcriptase	Sigma Aldrich	M1302
SuperScript indirect cDNA labeling core kit	Thermo Fischer	L101402
Cy3	GE Healthcare	GEPA13101
Cy5	GE Healthcare	GEPA15101
Critical Commercial Assays		
MasterPure Yeast DNA Purification Kit	Epicentre	MPY80200
Oligonucleotide Microarray	Agilent Technologies	Custom ordered
Deposited Data		
Sequence data of ChIP-exo experiments	This study	GSE84883
Microarray data of gene expression experiments	This study	GSE84883
Experimental Models: Organisms/Strains		
S. pombe standard laboratory strain (972) derivates	This study	See Table S1
Sequence-Based Reagents		
Primers	This study	See Table S2

(*Continued on next page*)

Continued

REAGENT or RESOURCE	SOURCE	IDENTIFIER
Software and Algorithms		
Bowtie 2	Langmead and Salzberg, 2012	http://bowtie-bio.sourceforge.net/bowtie2/index.shtml
Samtools	Li et al., 2009	http://samtools.sourceforge.net/
Bioconductor packages	N/A	https://www.bioconductor.org/
R	N/A	https://www.r-project.org/
Step One Software v2.3	Thermo Fischer	https://www.thermofisher.com/de/de/home/technical-resources/software-downloads/StepOne-and-StepOnePlus-Real-Time-PCR-System.html
Prism 7	GraphPad software	http://www.graphpad.com/scientific-software/prism/
Feature Extraction software	Agilent	http://www.genomics.agilent.com/en/Microarray-Scanner-Processing-Hardware/Feature-Extraction-Software/?cid=AG-PT-144&tabId=AG-PR-1050

CONTACT FOR REAGENT AND RESOURCE SHARING

Please direct any requests for further information or reagents to the lead contact, Associate Professor Tamás Fischer (tamas.fischer@anu.edu.au), Genome Biology Department, The John Curtin School of Medical Research, The Australian National University.

EXPERIMENTAL MODEL AND SUBJECT DETAILS

Schizosaccharomyces pombe strains used in this study are derivates of the standard laboratory strain 972 and are listed in Table S1.

METHOD DETAILS

DNA damage sensitivity assays

Wild-type and mutant cells were grown in YEA liquid media. An aliquot equivalent to 1 mL OD_{600} = 1 culture was removed from the culture, 5-fold serial dilutions were prepared, and the dilutions 5^{-1} to 5^{-7} were spotted onto freshly prepared YEA agar plates containing the indicated DNA damaging chemical (camptothecin: 150 μM; hydroxyurea: 5 mM; methyl methanesulfonate: 0.005) or without additional chemicals (Mock). For the UV-induced DNA damage, cells were first spotted onto YEA agar plates and then exposed to UV light (200 J/cm^3) using a Stratalinker (Stratagene) UV cross-linker.

Measuring the cleavage efficiency of I-PpoI

Cells were grown to exponential growth phase (30°C; YEA or SDC+/−thiamine for repression/induction of P*nmt1*-Rnh1 expression) and then diluted to an OD_{600} of 0.5. The endonuclease I-PpoI was induced by addition of 20 μg/ml anhydrotetracycline (ahTET, Sigma-Aldrich). Cell aliquots were taken pre- (OFF) and post- (ON) induction at indicated time points, and total genomic DNA was extracted (MasterPure Yeast DNA purification, Epicentre). Cleavage efficiency was assessed with PCR or qPCR (FAST SYBR Green Mix; Applied Biosystems) using primers spanning the I-PpoI cleavage site. Primers are listed in Table S2.

Measuring survival rate following I-PpoI or SmaI induction

Cells were grown in liquid media (30°C; YEA or SDC thiamine) to exponential growth phase, then diluted to an OD_{600} of 0.5 and split into two cultures. For one culture, 20 μg/ml ahTET was added for 2 hr to induce the endonuclease I-PpoI or 0.2 μg/ml ahTET was used to induce the endonuclease SmaI for 20 min. The other culture was left untreated as a control. Subsequently, cultures were 10-fold serial diluted up to 10^{-5} (in YEA or SDC thiamine) and 100 μl of every dilution was plated onto YEA or SDC+/− thiamine agar plates with glass beads (Roth). Plates were incubated for 2-4 days at 30°C until colonies formed. The relative survivor rate was determined as the number of surviving colonies relative to total colony number (I-PpoI/SmaI not induced). Values are shown as mean plus SEM of at least 3 biological replicates. p values were obtained using the two-tailed unpaired Student's t test.

Chromatin-immunoprecipitation ChIP)

Induction of double strand DNA breaks and cross linking

Cells were grown to exponential growth phase (30°C, YEA) and then diluted to an OD_{600} of 0.25 in YEA and split into two cultures. In one culture, 20 μg/mL ahTET was added, while the other culture was used as the non-induced control. Both were incubated at 30°C for the indicated times (+DSB and -DSB). With the exception of experiments using S9.6 antibody (RNA-DNA hybrid ChIP experiments), cells were cross-linked in 1 formaldehyde for 15 min at room temperature, pelleted (2600 rpm, 2 min), washed three times

in cold PBS and flash frozen. RNA-DNA hybrid ChIP pellets were pelleted, washed, and flash frozen, without formaldehyde cross-linking.

Cell lysis and sonication

Cells were lysed in lysis buffer (1 mg/ml Sodium-deoxycholate, 1 Triton-X, 0.05 M HEPES-KOH (pH 7.5), 0.14 M NaCl, 1 mM EDTA (pH 7.5), 1 mM PMSF, 1x Protease Inhibitor Cocktail (Serva)) and 700 µl 0.5 mm Zirconia beads (Roth) using Precellys 24 homogenizer (Bertin Instruments) 2x 5000 rpm for 20 s with 5 s pause. The lysate was collected and transferred to 1.5 mL TPX microtubes (Diagenode). The chromatin was sheared using the Bioruptor (Diagenode) with 30 cycles (30 s on, 30 s off) at 4°C, with the exception of RNA-DNA hybrid ChIP experiments (S9.6 antibody), where we used only 20 cycles. Samples were centrifuged and the ChIP extract (supernatant) was collected. Input samples represent 1.5 of the total ChIP extracts.

Immunoprecipitation and purification

DNA precipitation was carried out using anti-RNA-DNA hybrid antibody (S9.6, Kerafast) or anti-Pol II antibody (8WG16, Thermo Fischer) overnight at 4°C in the presence or absence (- ab sample) of 1 µl antibody (S9.6 – 0.5 µg/µl; 8WG16 – 2.5 µg/ml), followed by 2 hr incubation with 20µl (slurry) magnetic Protein A and Protein G beads mix (Millipore) at 4°C. ChIP experiments with Ssb2-Flag strains were directly incubated with 40 µl (slurry) anti-Flag M2 agarose beads (Sigma) for 2 hr at 4°C. Beads were washed twice in each of the following buffers: wash buffer I (1 mg/ml Sodium-deoxycholate, 1 Triton-X, 0.05 M HEPES-KOH (pH 7.5), 0.14 M NaCl, 1 mM EDTA (pH 7.5)), wash buffer II (1 mg/ml Sodium-deoxycholate, 1 Triton-X, 0.05 M HEPES-KOH (pH 7.5), 0.54 M NaCl, 1 mM EDTA (pH 7.5)), and wash buffer III (5 mg/ml Sodium-deoxycholate, 10 mM Tris (pH 8), 250 mM LiCl, 1 mM EDTA (pH 7.5), 1 NP-40). All washing steps were performed for 10 min at 4°C. Precipitated DNA was eluted in elution buffer (50 mM Tris (pH 8), 10 mM EDTA (pH 7.5), 1 SDS) for 2x 15 min at 65°C. Eluted samples were treated with RNase Cocktail (Thermo Fischer) for 2 hr at 37°C followed by proteinase K (Thermo Fischer) and reverse cross-linking overnight at 65°C. DNA was extracted with phenol:chloroform:isoamylalcohol (26:25:24, Roth).

Detection of enrichment by standard PCR

ChIP enrichment was checked using standard PCR techniques. Primers used are listed in Table S2. PCR products were visualized using the PhosphoImager FLA-7000 (Fujifilm) and intensities were quantified with AIDA Image Analyzer software. Enrichment was calculated as ChIP/Input with reference to either the –ab sample (S9.6) or the non-I-PpoI-induced sample.

ChIP-exo experiments

Starting material was collected from 250ml cultures at an OD_{660} of 0.8 and either washed and pelleted directly (RNA-DNA hybrid ChIP-exo) or crosslinked with 1 formaldehyde, and then washed and pelleted (Ssb2 ChIP-exo). ChIP-exo experiments were carried out as previously described (Rhee and Pugh, 2012) with some modifications. After the IP and wash steps (as described in the ChIP section), the following on-beads enzymatic reactions were carried out, with washing steps in between: The samples were treated with T4 DNA Polymerase (3U) for 20 min for blunt-ending, with T4 polynucleotide kinase (10U) for 30 min and with Klenow Fragment (3 5 exo-) (5U) for 30 min for 5 phosphorylation and A-tailing, respectively. The first adaptor ligation was performed overnight at 16°C with T4 DNA Ligase (500U). The samples were treated with T4 Polynucleotide Kinase (10U) for 30 min for 5 phosphorylation, then with Lambda Exonuclease (15U) for 6 min (S9.6 ChIP) or for 30 min (Ssb2 ChIP) to remove the 5 end of the adaptors. Ssb2 ChIP samples were also treated with RecJf exonuclease (45U) for 30 min. Samples were eluted in elution buffer containing 1 SDS, phenol-chloroform extracted and ethanol precipitated. The samples were then treated with phi29 DNA Polymerase (10U) for 20 min for blunt-ending and denatured for 10 min denaturation. Taq polymerase (2.5U) was used for A-tailing for 20 min. Samples were purified using 1.2x Ampure XP magnetic beads. A second adaptor ligation was performed overnight at 16°C with T4 DNA Ligase (500U). The resulting sequencing libraries were amplified, purified, and sequenced using Illumina HiSeq2000. Sequencing reads were mapped by Bowtie2 software (version 2.2.5) to a modified *S. pombe* genome (the artificial cut site added to chromosome II). Strand-specific coverage data were generated and the samples were normalized to total coverage on chromosome I using R Bioconductor packages.

qRT-PCR

Total RNA was treated with Turbo DNase (Life Technologies) and 100 ng was reverse transcribed with random hexamers, followed by qPCR (SensiFast SYBR Hi ROX One Step Kit).

Microarray experiments

Microarray experiments were carried out as previously described (Zhou et al., 2015) with some minor modifications: WT and mutant strains were grown in YEA (WT and *rnh1 rnh201*) or SDC-Th (P*nmt1*-Rnh1 ON) or SDC+Th (P*nmt1*-Rnh1 OFF) at 30°C to an OD_{600} of 0.6. Total RNAs from WT and mutants were isolated using TRI Reagent (Sigma Aldrich) followed by reverse transcription using the SuperScript Indirect cDNA labeling system (Life Technologies) with anchored oligo$(dT)_{20}$. cDNAs from WT and P*nmt1*-Rnh1 OFF strains were labeled with Cy3 (GE Healthcare); *rnh1 rnh201* and P*nmt1*-Rnh1 ON strains were labeled with Cy5 (GE Healthcare); labeled cDNAs were hybridized to high-resolution tiling microarrays (Agilent) consisting of forward- and reverse-DNA-strand-specific probes. Expression arrays were performed in two biological replicates.

QUANTIFICATION AND STATISTICAL ANALYSIS

Statistical parameters are reported in the Figures and the Figure Legends.

DATA AND SOFTWARE AVAILABILITY

The accession number for the raw data files and processed WIG files for Sequence data of ChIP-exo experiments and the microarray data of gene expression experiments is deposited in NCBI GEO under the reference number GEO: GSE84883.

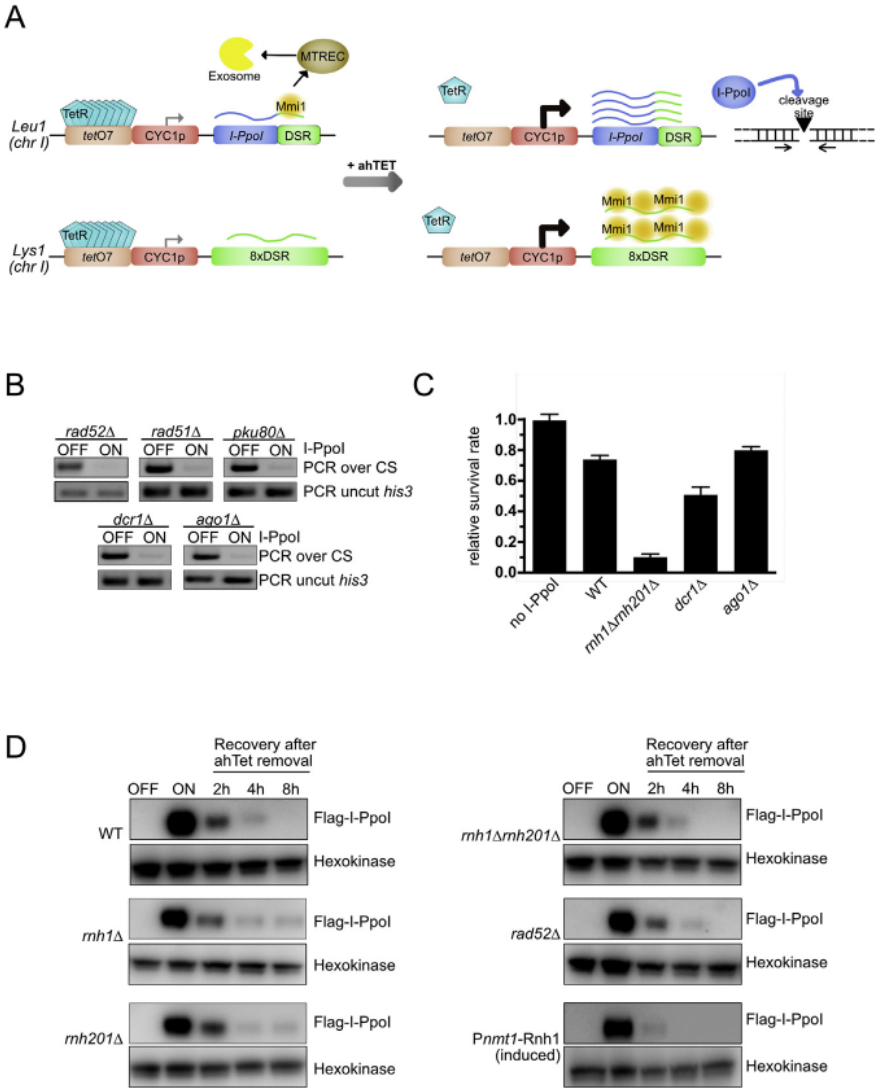

Figure S1. I-PpoI-Induced Site-Specific DSB System Used in This Study Related to Figure 1

(A) Schematic depicting the I-PpoI induced DSB system used in the study. The endonuclease I-PpoI and the ncRNA containing 8 copies of the DSR (**d**eterminant of **s**elective **r**emoval) sequences are under the control of a tetracycline-inducible CYC1 promoter (CYC1p), and in the absence of tetracycline, the expression of the I-PpoI and the ncRNA-8xDSR is repressed by the tetracycline repressor (TetR-tup11). In order to eliminate trace amounts of background expression of I-PpoI, a DSR sequence was incorporated into the 3 UTR of the I-PpoI gene. DSR sequences are recognized by the Mmi1 protein, which directs the transcripts through the MTREC complex to the nuclear exosome for rapid degradation. Upon induction of the system with anhydrotetracyline, TetR is released from the promoter and the expression of I-PpoI and ncRNA-8xDSR is rapidly induced. The high level of ncRNA-8xDSR competes for the Mmi1 proteins and stabilizes the I-PpoI transcripts and allows nucleo-cytoplasmic export and translation to I-PpoI protein, which then cleaves dsDNA at its target sites.

(B) I-PpoI cleavage efficiency is similar in all I-PpoI-expressing strains. PCR amplification was performed on genomic DNA from the indicated strains pre- (OFF) and post- (ON) I-PpoI induction using primers spanning the cleavage site at *chr II* (PCR over CS) and primers in the *his3* locus as a control (PCR uncut *his3*). Data for additional mutant strains are shown in Figure 1C.

(C) Deletion of RNAi factors only slightly influence survival following I-PpoI-induced DNA damage. I-PpoI expression was induced for 2h (each strain also had a non-induced control), and cells were then plated under non- I-PpoI-inducing conditions. Surviving colonies were counted after 2 days. Relative survivor rate for each strain represents the number of survivors in the I-PpoI-induced sample relative to the non-induced control. Data are represented as mean + SEM of at least 3 biological replicates.

(D) I-PpoI protein levels are comparable between WT and indicated mutant strains. Western-blot was performed using anti-Flag antibody (detecting Flag-I-PpoI protein) and anti-hexokinase antibody as a control. I-PpoI was not induced (OFF) or induced for 2h (ON) and subsequently I-PpoI induction was stopped by the removal of ahTET (t = 0h) and the level of Flag-I-PpoI was monitored at the indicated time-points.

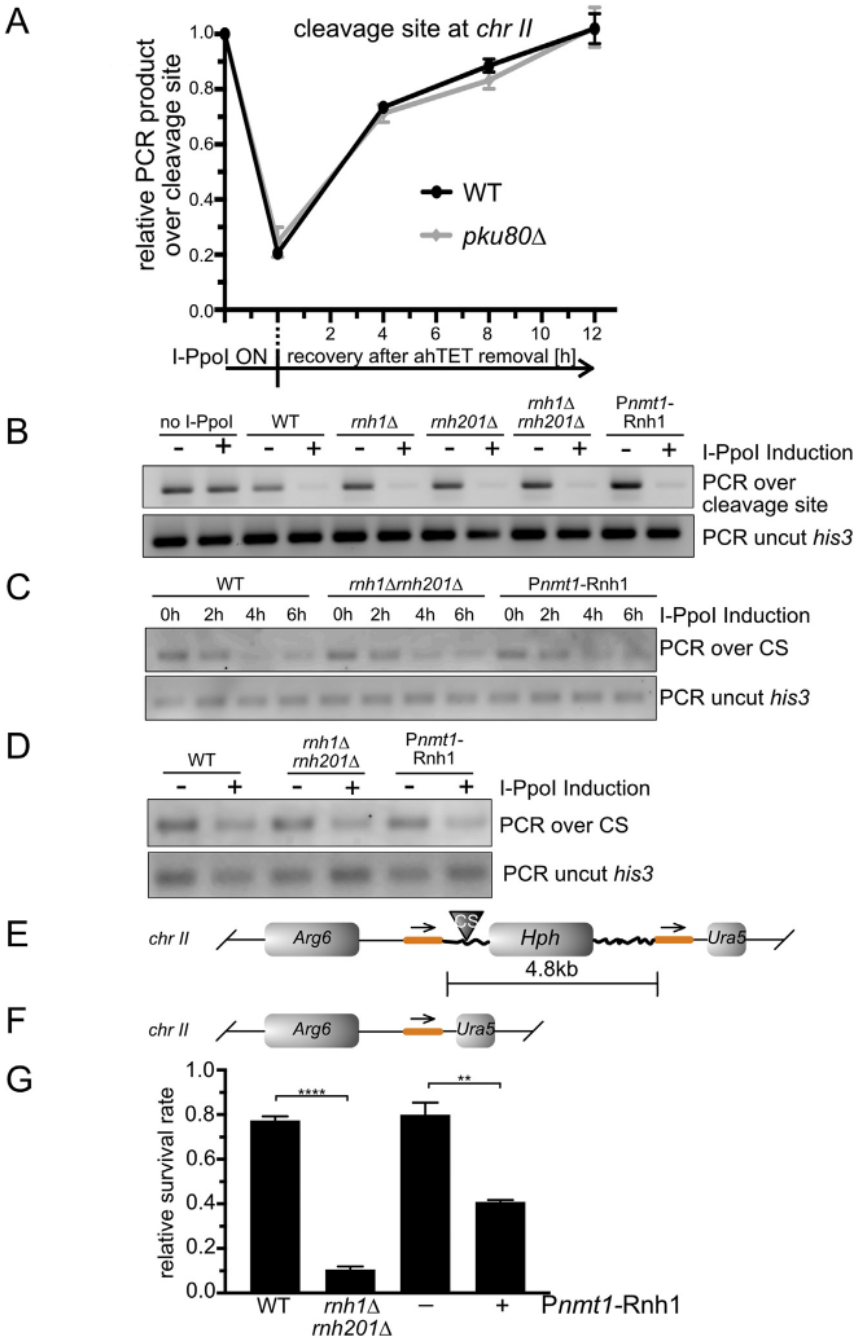

Figure S2. Deletion or Over-Expression of RNase H Impairs DSB Repair in the Presence or Absence of Damage at the rDNA Repeats Related to Figures 1D and 1E

(A) Cleavage and recovery of the I-PpoI cleavage site at *chr II* in the *pku80* mutant. For additional mutants, see Figure 1E. qPCR was performed using primers spanning the cleavage site. Data are presented as relative qPCR signal compared to the non-cleaved sample (pre-I-PpoI induction) in the indicated strains. I-PpoI was induced for 2h and I-PpoI induction was stopped by the removal of ahTET (t = 0h) and the repair efficiency was measured at the indicated time-points. Data are represented as mean SEM of 3 biological replicates.

(B) Controls for cleavage efficiency for strains assessed in Figure 2A.

(C) Controls for cleavage efficiency for strains assessed in Figure 4A.

(D) Controls for cleavage efficiency for strains assessed in Figure 4B.

(E) Schematic depicting the I-PpoI cleavage site at *chr II* in the P*nmt1*-Rnh1-*Hph* strain (related to Figure 5E). 500 bp long direct repeats (orange line) flank a 4.8 kb unique DNA sequence (thick wavy line) including the I-PpoI cleavage site (CS) and the hygromycin phosphotransferase gene (*Hph*).

(F) Schematic depicting the genomic region around the I-PpoI cleavage site in 10 randomly chosen hygromycin sensitive colonies from the experiment presented in Figure 5E.

legend continued on next page)

(G) Double-deletion of *rnh1* and *rnh201* or overexpression of Rnh1 leads to impaired survival following SmaI-induced DSBs (related to Figure 1D). SmaI expression was induced for 20 min (each strain also had a non-induced control), and cells were plated under non- SmaI-inducing conditions. Surviving colonies were counted after 2 days and replica plated to SmaI inducing media (YEA+20 μg/ml Dox) to monitor escape mutants that lost the functional SmaI gene. Relative survival rate for each strain represents the number of surviving cells in the SmaI-induced sample (after subtracting the number of escape mutants) relative to the non-induced control. For the P*nmt1*-Rnh1 strain, overexpression of Rnh1 is indicated (+). Data are represented as mean + SEM of at least 3 biological replicates. p values were obtained using the two-tailed unpaired Student's t test (**p 0.01; ****p 0.0001).